

Analysis of Diffractive Optical Neural Networks and Their Integration with Electronic Neural Networks

Deniz Mengü^{1,2,3†}, Yi Luo^{1,2,3†}, Yair Rivenson^{1,2,3}, Aydogan Ozcan^{1,2,3,4,}*

¹ Electrical and Computer Engineering Department, University of California, Los Angeles, CA, 90095, USA

² Bioengineering Department, University of California, Los Angeles, CA, 90095, USA

³ California NanoSystems Institute, University of California, Los Angeles, CA, 90095, USA

⁴ Department of Surgery, David Geffen School of Medicine, University of California, Los Angeles, CA, 90095, USA.

†Equal contributing authors.

*Email: ozcan@ucla.edu

Keywords: Optical computing, Deep networks, Deep learning, All-optical neural networks, Hybrid neural networks

ABSTRACT

Optical machine learning offers advantages in terms of power efficiency, scalability and computation speed. Recently, an optical machine learning method based on diffractive deep neural networks (D²NNs) has been introduced to execute a function as the input light diffracts through passive layers, designed by deep learning using a computer. Here we introduce

improvements to D^2NN s by changing the training loss function and reducing the impact of vanishing gradients in the error back-propagation step. Using five phase-only diffractive layers, we numerically achieved a classification accuracy of 97.18% and 87.67% for optical recognition of handwritten digits and fashion products, respectively; using both phase and amplitude modulation (complex-valued) at each layer, our inference performance improved to 97.81% and 88.76%, respectively. Furthermore, we report the integration of D^2NN s with electronic neural networks to create hybrid classifiers that significantly reduce the number of input pixels into an electronic network using an ultra-compact front-end D^2NN with a layer-to-layer distance of a few wavelengths, also reducing the complexity of the successive electronic network. Using a 5-layer phase-only D^2NN jointly-optimized with a single fully-connected electronic layer, we achieved a classification accuracy of 98.17% and 89.90% for the recognition of handwritten digits and fashion products, respectively. Moreover, the input to the electronic network was compressed by >7.8 times down to 10×10 pixels, making the jointly-optimized hybrid system perform classification with a simple electronic layer. Beyond creating low-power and high-frame rate ubiquitous machine learning platforms, such D^2NN -based hybrid neural networks will find applications in optical imager and sensor design.

INTRODUCTION

Optics in machine learning has been widely explored due to its unique advantages, encompassing power efficiency, speed and scalability¹⁻³. Some of the earlier work include optical implementations of various neural network architectures⁴⁻¹¹, with a recent resurgence¹²⁻²², following the availability of powerful new tools for applying deep neural networks^{23,24}, which have redefined the state-of-the-art for a variety of machine learning tasks. In this line of work, we have recently introduced an optical machine learning framework, termed as Diffractive Deep Neural Network (D^2NN)¹⁵, where deep learning and error back-propagation methods are used to design, using a computer, diffractive layers that collectively perform a desired task that the network is trained for. In this training phase of a D^2NN , the transmission and/or reflection coefficients of the individual pixels (i.e., neurons) of each layer are optimized such that as the light diffracts from the input plane toward the output plane, it computes the task at hand. Once this training phase in a computer is complete, these passive layers can be physically fabricated and stacked together to form an all-optical network that executes the trained function without the use of any power, except for the illumination light and the output detectors.

In our previous work, we experimentally demonstrated the success of D^2NN framework at THz part of the electromagnetic spectrum and used a standard 3D-printer to fabricate and assemble together the designed D^2NN layers¹⁵. In addition to demonstrating optical classifiers, we also demonstrated that the same D^2NN framework can be used to design an imaging system by 3D-engineering of optical components using deep learning¹⁵. In these earlier results, we used coherent illumination and encoded the input information in phase or amplitude channels of different D^2NN systems. Another important feature of D^2NN s is that the axial spacing between

the diffractive layers is very small, e.g., less than 50 wavelengths (λ)¹⁵, which makes the entire design highly compact and flat.

Our experimental demonstration of D²NNs was based on linear materials, without including the equivalent of a nonlinear activation function within the optical network; however, as detailed in Ref. 15, optical nonlinearities can also be incorporated into a D²NN using non-linear materials including e.g., crystals, polymers or semiconductors, to further improve its inference performance using nonlinear optical effects within diffractive layers. For such a nonlinear D²NN design, resonant nonlinear structures (based on e.g., plasmonics or metamaterials) tuned to the illumination wavelength could be important to lower the required intensity levels. Even using linear optical materials to create a D²NN, the optical network designed by deep learning shows “*depth*”, i.e., a single diffractive layer does not possess the same degrees-of-freedom to achieve the same level of classification accuracy, power efficiency and signal contrast at the output plane that multiple diffractive layers can collectively achieve for a given task. It is true that, for a linear diffractive optical network, the entire wave propagation and diffraction phenomena that happen between the input and output planes can be squeezed into a single matrix operation; *however*, this arbitrary mathematical operation defined by multiple learnable diffractive layers cannot be performed in general by a single diffractive layer placed between the same input and output planes. That is why, multiple diffractive layers forming a D²NN show the *depth* advantage and statistically perform better compared to a single diffractive layer trained for the same classification task, and achieve improved accuracy as also discussed in the supplementary materials of Ref. 15.

Here, we present a detailed analysis of D²NN framework, covering different parameters of its design space, also investigating its depth advantage, and provide significant improvements to its

inference performance by changing the loss function involved in the training phase, and reducing the effect of vanishing gradients in the error back-propagation step through its layers. To provide examples of its improved inference performance, using a 5-layer D^2NN design (Figure 1), we optimized two different classifiers to recognize (1) hand-written digits, 0 through 9, using the MNIST (Mixed National Institute of Standards and Technology) image dataset²⁵, and (2) various fashion products, including t-shirts, trousers, pullovers, dresses, coats, sandals, shirts, sneakers, bags, and ankle boots (using the Fashion MNIST image dataset²⁶). These 5-layer phase-only all-optical diffractive networks achieved a numerical blind testing accuracy of 97.18% and 87.67% for hand-written digit classification and fashion product classification, respectively. Using the same D^2NN design, this time with both the phase and the amplitude of each neuron's transmission as learnable parameters (which we refer to as *complex-valued* D^2NN design), we improved the inference performance to 97.81% and 88.76% for hand-written digit classification and fashion product classification, respectively. We also provide comparative analysis of D^2NN performance as a function of our design parameters, covering the impact of the number of layers, layer-to-layer connectivity and loss function used in the training phase on the overall classification accuracy, output signal contrast and power efficiency of D^2NN framework.

Furthermore, we report the integration of D^2NN s with electronic neural networks to create hybrid machine learning and computer vision systems. Such a hybrid system utilizes a D^2NN at its front-end, before the electronic neural network, and if it is jointly optimized (i.e., optical and electronic as a monolithic system design), it presents several important advantages. This D^2NN -based hybrid approach can all-optically *compress* the needed information by the electronic network using a D^2NN at its front-end, which can then significantly reduce the number of pixels (detectors) that needs to be digitized for an electronic neural network to act on. This would

further improve the frame-rate of the entire system, also reducing the complexity of the electronic network and its power consumption. This D^2NN -based hybrid design concept can potentially create ubiquitous and low-power machine learning systems that can be realized using relatively simple and compact imagers, with e.g., a few tens to hundreds of pixels at the opto-electronic sensor plane, preceded by an ultra-compact all-optical diffractive network with a layer-to-layer distance of a few wavelengths, which presents important advantages compared to some other hybrid network configurations involving e.g., a 4-f configuration¹⁶ to perform a convolution operation before an electronic neural network.

To better highlight these unique opportunities enabled by D^2NN -based hybrid network design, we conducted an analysis to reveal that a 5-layer phase-only (or *complex-valued*) D^2NN that is jointly-optimized with a single fully-connected layer, following the optical diffractive layers, achieves a blind classification accuracy of 98.17% (or 98.51%) and 89.90% (or 89.60%) for the recognition of hand-written digits and fashion products, respectively. In these results, the input image to the electronic network (created by diffraction through the jointly-optimized front-end D^2NN) was also compressed by more than 7.8 times, down to 10×10 pixels, which confirms that a D^2NN -based hybrid system can perform competitive classification performance even using a relatively simple and one-layer electronic network that uses significantly reduced number of input pixels.

In addition to potentially enabling ubiquitous, low-power and high-frame rate machine learning and computer vision platforms, these hybrid neural networks which utilize D^2NN -based all-optical processing at its front-end will find other applications in the design of compact and ultra-thin optical imaging and sensing systems by merging fabricated D^2NN s with opto-electronic sensor arrays. This will create intelligent systems benefiting from various CMOS/CCD imager

chips and focal plane arrays at different parts of the electromagnetic spectrum, merging the benefits of all-optical computation with simple and low-power electronic neural networks that can work with lower dimensional data, all-optically generated at the output of a jointly-optimized D²NN design.

RESULTS AND DISCUSSION

Mitigating vanishing gradients in optical neural network training

In D²NN framework, each neuron has a complex transmission coefficient, i.e., $t_i^l(x_i, y_i, z_i) = a_i^l(x_i, y_i, z_i) \exp(j\phi_i^l(x_i, y_i, z_i))$, where i and l denote the neuron and diffractive layer number, respectively. In Ref. 15, a_i^l and ϕ_i^l are represented during the network training as two latent variables, α and β , in the following form:

$$a_i^l = \text{sigmoid}(\alpha_i^l), \quad (1a)$$

$$\phi_i^l = 2\pi \times \text{sigmoid}(\beta_i^l), \quad (1b)$$

where, $\text{sigmoid}(x) = \frac{e^x}{e^x + 1}$, is a non-linear activation function. Note that in eq. (1), the sigmoid acts on an auxiliary variable rather than the information flowing through the network. Being a bounded analytical function, sigmoid confines the values of a_i^l and ϕ_i^l inside the intervals (0,1) and (0,2 π), respectively. On the other hand, it is known that sigmoid function has vanishing gradient problem²⁷ due to its relatively flat tails, and when it is used in the context depicted in eq. (1), it can prevent the network to utilize the available dynamic range considering both the

amplitude and phase terms of each neuron. To mitigate these issues, in this work we replaced eq. (1) as follows:

$$a_i^l = \frac{\text{ReLU}(\alpha_i^l)}{\max_{0 < i < M} \{\text{ReLU}(\alpha_i^l)\}}, \quad (2a)$$

$$\phi_i^l = 2\pi \times \beta_i^l. \quad (2b)$$

where ReLU refers to Rectified Linear Unit, and M is the number of neurons per layer. Based on eq. (2), the phase term of each neuron, ϕ_i^l , becomes unbounded, but since the $\exp(j\phi_i^l(x_i, y_i, z_i))$ term is periodic (and bounded) with respect to ϕ_i^l , the error back-propagation algorithm is able to find a solution for the task in hand. The amplitude term, a_i^l , on the other hand, is kept within the interval (0,1) by using an explicit normalization step shown in eq. (2).

To exemplify the impact of this change *alone* in the training of an all-optical D²NN design, for a 5-layer, phase-only (*complex-valued*) diffractive optical network with an axial distance of $40 \times \lambda$ between its layers, the classification accuracy for Fashion-MNIST dataset increased from reported 81.13% (86.33%) to 85.40% (86.68%) following the above discussed changes in the parameterized formulation of the neuron transmission values compared to earlier results in Ref. 15. We will report further improvements in the inference performance of an all-optical D²NN after the introduction of the loss function related changes into the training phase, which is discussed next.

Effect of the learning loss function on the performance of all-optical diffractive neural networks

Earlier work on D²NNs¹⁵ reports the use of mean squared error (MSE) loss. An alternative loss

function that can be used for the design of a D^2NN is the cross-entropy loss²⁸⁻³⁰ (see the Methods section). Since minimizing the cross-entropy loss is equivalent to minimizing the negative log-likelihood (or maximizing the likelihood) of an underlying probability distribution, it is in general more suitable for classification tasks. Note that, cross-entropy acts on probability measures, which take values in the interval (0,1) and the signals coming from the detectors (one for each class) at the output layer of a D^2NN are not necessarily in this range; therefore, in the training phase, a *softmax* layer is introduced to be able to use the cross-entropy loss. It is important to note that although *softmax* is used during the training process of a D^2NN , once the diffractive design converges and is fixed, the class assignment at the output plane of a D^2NN is still based *solely on the maximum optical signal detected at the output plane*, where there is one detector assigned for each class of the input data (see Figures 1A, 1F).

When we combine D^2NN training related changes reported in the earlier sub-section on the parametrization of neuron modulation (eq. (2)), with the cross-entropy loss outlined above, a significant improvement in the classification performance of an all-optical diffractive neural network is achieved. For example, for the case of a 5-layer, phase-only D^2NN with $40 \times \lambda$ axial distance between the layers, the classification accuracy for MNIST dataset increased from 91.75% to 97.18%, which further increased to 97.81% using complex-valued modulation, treating the phase and amplitude coefficient of each neuron as a learnable parameter. The training convergence plots and the confusion matrices corresponding to these results are also reported in Figures 2A and 2C, for phase-only and complex-valued modulation cases, respectively. Similarly, for Fashion-MNIST dataset, we improved the blind testing classification accuracy of a 5-layer phase-only (*complex-valued*) D^2NN from 81.13% (86.33%) to 87.67% (88.76%), showing a similar level of advancement as in the MNIST results. Figures 3A and 3C

also report the training convergence plots and the confusion matrices for these improved Fashion-MNIST inference results, for phase-only and complex-valued modulation cases, respectively. As a reference point, a fully-electronic deep neural network such as ResNet³¹ (with >25 Million learnable parameters) achieves 99.51% and 93.23% for MNIST and Fashion-MNIST datasets, respectively, which are superior to our 5-layer all-optical D^2NN inference results (i.e., 97.81% and 88.76% for MNIST and Fashion-MNIST datasets, respectively), which in total used 0.8 million learnable parameters, covering the phase and amplitude values of the neurons at 5 successive diffractive layers.

All these results demonstrate that the D^2NN framework using linear optical materials can already achieve a decent classification performance, also highlighting the importance of future research on the integration of optical nonlinearities into the layers of a D^2NN , using e.g., plasmonics, metamaterials or other nonlinear optical materials (see the supplementary information of Ref. 15), in order to come closer to the performance of state-of-the-art digital deep neural networks.

Performance trade-offs in D^2NN design

Despite the significant increase observed in the blind testing accuracy of D^2NN s, the use of softmax-cross-entropy (SCE) loss function in the context of all-optical networks also presents some trade-offs in terms of practical system parameters. MSE loss function operates based on pixel-by-pixel comparison of a user-designed output distribution with the output optical intensity pattern, after the input light interacts with the diffractive layers (see e.g., Figures 1D and 1I). On the other hand, SCE loss function is much less restrictive for the pixel-by-pixel distribution of the output intensity behind the diffractive layers (see e.g., Figures 1E and 1J); therefore it

presents additional degrees-of-freedom and redundancy for the diffractive network to improve its inference accuracy for a given machine learning task, as reported in the earlier sub-section.

This performance improvement with the use of SCE loss function in a diffractive neural network design comes at the expense of some compromises in terms of the expected diffracted power efficiency and signal contrast at the network output. To shed more light on this trade-off, we define the power efficiency of a D^2NN as the percentage of the optical signal detected at the target label detector (I_L) corresponding to the correct data class with respect to the *total* optical signal at the output plane of the optical network (E). Figure 4B and Figure 4E show the power efficiency comparison as a function of the number of diffractive layers (corresponding to 1, 3 and 5-layer phase-only D^2NN designs) for MNIST and Fashion-MNIST datasets, respectively. The power efficiency values in these graphs were computed as the ratio of the mean values of I_L and E for the test samples that were correctly classified by the corresponding D^2NN designs (refer to Figures 4A and 4D for the classification accuracy of each design). These results clearly indicate that increasing the number of diffractive layers has significant positive impact on the optical efficiency of a D^2NN , regardless of the loss function choice. The maximum efficiency that a 5-layer phase-only D^2NN design based on the SCE loss function can achieve is 1.98% for MNIST and 0.56% for Fashion-MNIST datasets, which are significantly lower compared to the efficiency values that diffractive networks designed with MSE loss function can achieve, i.e., 25.07% for MNIST and 26.00% for Fashion-MNIST datasets (see Figures 4B and 4E). Stated differently, MSE loss function based D^2NN s are in general significantly more power efficient all-optical machine learning systems.

Next we analyzed the signal contrast of diffractive neural networks, which we defined as the difference between the optical signal captured by the target detector (I_L) corresponding to the

correct data class and the maximum signal detected by the rest of the detectors (i.e., the strongest competitor (I_{SC}) detector for each test sample), normalized with respect to the total optical signal at the output plane (E). The results of our signal contrast analysis are reported in Figure 4C and Figure 4F for MNIST and Fashion-MNIST datasets, respectively, which reveal that D²NNs designed with an MSE loss function keep a strong margin between the target detector (I_L) and the strongest competitor detector (among the rest of the detectors) at the output plane of the all-optical network. The minimum mean signal contrast value observed for an MSE-based D²NN design was for a 1-Layer, phase-only diffractive design, showing a mean signal contrast of 2.58% and 1.37% for MNIST and Fashion-MNIST datasets, respectively. Changing the loss function to SCE lowers the overall signal contrast of diffractive neural networks as shown in Figures 4C and 4F.

Comparing the performances of MSE-based and SCE-based D²NN designs in terms of classification accuracy, power efficiency and signal contrast, as depicted in Figure 4, we identify two opposite design strategies in diffractive all-optical neural networks. MSE, being a strict loss function acting in the physical space (e.g., Figures 1D and 1I), promotes high signal contrast and power efficiency of the diffractive system, while SCE, being much less restrictive in its output light distribution (e.g., Figures 1E and 1J), enjoys more degrees-of-freedom to improve its inference performance for getting better classification accuracy, at the cost of a reduced overall power efficiency and signal contrast at its output plane.

Is D²NN framework shallow or deep?

As demonstrated in Figure 4, multiple diffractive layers that collectively operate within a D²NN design present additional degrees-of-freedom compared to a single diffractive layer to achieve

better classification accuracy, as well as improved diffraction efficiency and signal contrast at the output plane of the network; the latter two are especially important for experimental implementations of all-optical diffractive networks as they dictate the required illumination power levels as well as signal-to-noise ratio related error rates for all-optical classification tasks. Stated differently, D^2NN framework, even when it is composed of linear optical materials, is “Deep” and shows “Depth” advantage because an increase in the number of diffractive layers (1) improves its statistical inference accuracy (see Figs. 4A and 4D), and (2) improves its overall power efficiency and the signal contrast at the correct output detector with respect to the detectors assigned to other classes (see Figs. 4B,C,E,F). Therefore, for a given input illumination power and detector signal-to-noise ratio, the overall error rate of the all-optical network decreases as the number of diffractive layers increase. All these highlight the depth feature of a D^2NN .

This is not in contradiction with the fact that, for an all-optical D^2NN that is made of linear optical materials, the entire diffraction phenomenon that happens between the input and output planes can be squeezed into a single matrix operation (in reality, every material exhibits some volumetric and surface nonlinearities, and what we mean here by a linear optical material is that these effects are negligible). In fact, such an arbitrary mathematical operation defined by multiple learnable diffractive layers cannot be performed in general by a single diffractive layer placed between the same input and output planes; additional optical components/layers would be needed to all-optically perform an arbitrary mathematical operation that multiple learnable diffractive layers can in general perform. Our D^2NN framework creates a unique opportunity to use deep learning principles to design multiple diffractive layers, within a very tight layer-to-layer spacing of less than $50\times\lambda$, that collectively function as an all-optical classifier, and this

framework will further benefit from nonlinear optical materials¹⁵ and resonant optical structures to further enhance its inference performance.

In addition to the above highlighted *depth/deepness* feature of a D²NN, another strong connection between deep learning and the D²NN framework is the fact that standard deep learning tools available in e.g., TensorFlow are at the heart of 3D engineering of D²NN layers to all-optically execute machine learning tasks, which forms the basis of D²NNs and one of the core teachings of Ref. 15.

Connectivity in diffractive neural networks

In a D²NN design, the layer-to-layer connectivity of the optical network is controlled by several parameters: the axial distance between the layers (Δ_z), the illumination wavelength (λ), the size of each neuron and the width of the diffractive layers. In our numerical simulations, we used a neuron size of approximately $0.53 \times \lambda$. In addition, the height and width of each diffractive layer was set to include $200 \times 200 = 40K$ neurons per layer. In this arrangement, if the axial distance between the successive diffractive layers is set to be $\sim 40 \times \lambda$ as in Ref. 15, then our D²NN design becomes fully-connected. On the other hand, one can also design a much thinner and more compact diffractive network by reducing Δ_z at the cost of limiting the connectivity between the diffractive layers. To evaluate the impact of this reduction in network connectivity on the inference performance of a diffractive neural network, we tested the performance of our D²NN framework using $\Delta_z = 4 \times \lambda$, i.e., 10-fold thinner compared to our earlier discussed diffractive networks. With this partial connectivity between the diffractive layers, the blind testing accuracy for a 5-layer, phase-only D²NN decreased from 97.18% ($\Delta_z = 40 \times \lambda$) to 94.12%

($\Delta_z = 4 \times \lambda$) for MNIST dataset (see Figures 2A and 2B, respectively). However, when the optical neural network with $\Delta_z = 4 \times \lambda$ was relaxed from phase-only modulation constraint to full complex modulation, the classification accuracy increased to 96.01% (Figure 2D), partially compensating for the lack of full-connectivity. Similarly, for Fashion-MNIST dataset, the same compact architecture with $\Delta_z = 4 \times \lambda$ provided accuracy values of 85.98% and 88.54% for phase-only and complex-valued modulation schemes, as shown in Figures 3B and 3D, respectively, demonstrating the vital role of phase and amplitude modulation capability for partially-connected, thinner and more compact optical networks.

Integration of diffractive neural networks with electronic networks: Performance analysis of D^2NN -based hybrid machine learning systems

Integration of passive diffractive neural networks with electronic neural networks (see e.g., Figures 5A and 5C) creates some unique opportunities to achieve pervasive and low-power machine learning systems that can be realized using simple and compact imagers, composed of e.g., a few tens to hundreds of pixels per opto-electronic sensor frame. To investigate these opportunities, for both MNIST (Table 1) and Fashion-MNIST (Table 2) datasets, we combined our D^2NN framework (as an all-optical *front-end*, composed of 5 diffractive layers) with 4 different electronic neural networks considering various sensor resolution scenarios as depicted in Table 3. For the electronic neural networks that we considered in this analysis, in terms of complexity and the number of trainable parameters, a single fully-connected digital layer and a custom designed 4-layer convolutional neural network (CNN) (see Table 4) represent the lower end of the spectrum, whereas, LeNet and ResNet represent some of the well-established and

proven deep neural networks with more advanced architectures and considerably higher number of trainable variables (Table 3). All these digital networks used in our analysis, were individually placed after both a fully-connected ($\Delta_Z = 40 \times \lambda$) and a partially-connected ($\Delta_Z = 4 \times \lambda$) D^2NN design and the entire hybrid system in each case was *jointly* optimized.

Among the all-optical D^2NN -based classifiers presented in the previous sections, fully-connected ($\Delta_Z = 40 \times \lambda$) complex modulation D^2NN designs have the highest classification accuracy values, while, partially-connected ($\Delta_Z = 4 \times \lambda$) designs with phase-only restricted modulation are at the bottom of the performance curve (see the all-optical parts of Tables 1 and 2). Hybrid systems with D^2NN designs at their front-end, however, perform almost at the same level for both the fully-connected complex modulation D^2NN designs and the partially-connected phase-only D^2NN designs, especially for the low pixel-count opto-electronic arrays, reported in the 2nd, 3rd and 4th rows of Tables 1 and 2. For example, for the hybrid system with a 10×10 detector array at the output plane of the optical network, a single fully-connected electronic layer can make up for some of the limitations (e.g., partial connectivity or restrictions on the neuron modulation function) of the D^2NN optical front-end design. Moreover, when the number of opto-electronic detectors is further increased as shown in the 3rd and 4th rows of Tables 1 and 2, the performance of the hybrid systems increases up to a certain level, regardless of the physical constraints on the modulation and connectivity of the optical front-end D^2NN s. Considering the importance of compact, thin and low-power designs, D^2NN -based hybrid systems with only tens to hundreds of pixels and an ultra-thin all-optical D^2NN front-end with a layer-to-layer distance of a few wavelengths (e.g., $4 \times \lambda$) cast a highly sought design to extend the applications of jointly-trained opto-electronic machine learning systems to various fields, without sacrificing the performance.

Focusing on the *all-electronic* parts of Tables 1 and 2, one can immediately notice that relatively simple neural networks (e.g., single fully-connected layer and 4-layer CNN) perform considerably worse compared to LeNet and ResNet, as expected. In fact, these simple neural networks also perform much worse than an all-optical D²NN design; for example a 5-layer complex-valued D²NN design achieves accuracy levels of 97.81% and 88.76% for MNIST and Fashion-MNIST datasets, respectively, whereas a 4-layer CNN (Table 4) achieves 95.08% and 81.76% for the same datasets, respectively (see Tables 1 and 2, all-optical vs. all-electronic). However, when these simple electronic networks are combined and jointly trained with a passive D²NN at their front-end, the classification performance of the hybrid system increases significantly, even with ~ 7.8 times reduced number of input pixels (i.e., 10×10 pixels compared to the raw data, 28×28 pixels), almost matching the results of LeNet, which has a more complex digital architecture, and would consume more power to operate compared to a single fully-connected layer or a 4-layer CNN. For example, a 5-layer phase-only D²NN design with $\Delta_z = 4 \times \lambda$ and 10×10 output detectors, jointly-optimized with a single fully-connected electronic layer achieves a classification accuracy of 98.17% and 89.90% for MNIST and Fashion-MNIST datasets, respectively; for the same datasets, a single fully-connected electronic layer *alone*, acting on 28×28 input pixels, achieves a classification accuracy 91.68% and 83.65%, respectively, once again highlighting the performance advantage of the D²NN-based hybrid system (see Tables 1 and 2). For further comparison, LeNet alone (acting on 32×32 pixels, up-sampled from raw data: 28×28 pixels) achieves 98.77% and 90.27% for MNIST and Fashion-MNIST datasets, respectively (see Tables 1 and 2). These results highlight that D²NN-based hybrid networks provide all-optical compression, permitting the use of much fewer pixels at the opto-electronic detector layer that feeds the electronic neural network, and enable the use of

simple electronic networks with significantly reduced number of trainable parameters (Table 3), while also getting competitive in their inference performance.

Jointly optimizing our D²NN framework with more sophisticated convolutional neural networks such as LeNet and ResNet did not result in further improvement (see the 3rd and 4th columns in Tables 1 and 2). In fact, their classification performance was observed to be higher without an optical network as shown in Tables 1 and 2. These results suggest that such advanced electronic neural networks are not suitable to be jointly-optimized with D²NNs when the opto-electronic sensor-array bonding the two parts of the hybrid system is monochrome and limited in terms of its space-bandwidth product. One hypothesis could be that while modern electronic deep neural networks present the current state of the art in computer vision, they are optimized to handle signals that result from color imaging systems, which were primarily designed to maximize the amount of information as perceived by a human observer. As future research, it is worth to explore novel D²NN-based color network architectures that will fully exploit the potentials of such opto-electronic hybrid systems.

METHODS

Diffractive neural network architecture

In our simulations, input objects were encoded in amplitude channel (MNIST) or phase channel (Fashion-MNIST) of the input plane, and were illuminated with a uniform plane wave at a wavelength of λ . In this manuscript, input plane represents the plane of the input object or its data, which can also be generated by another optical imaging system or a lens, e.g., by projecting an image of the object data. Optical fields at each plane were sampled on a grid with a spacing of

$\sim 0.53\lambda$ in both x and y directions. Between two diffractive layers, the free-space propagation was calculated using the angular spectrum method¹⁵. Each diffractive layer, with a neuron size of $0.53\lambda \times 0.53\lambda$, modulated the incident light in phase and/or amplitude, where the modulation value was a trainable parameter and the modulation method (phase-only or complex) was a pre-defined design parameter of the network. The number of layers and the axial distance from the input plane to the first diffractive layer, between the successive diffractive layers, and from the last diffractive layer to the detector plane were also pre-defined design parameters. At the detector plane, the output field intensity was calculated.

Forward propagation model

Following the Rayleigh-Sommerfeld equation³², a single neuron can be considered as the secondary source of wave $w_i^l(x, y, z)$, which is given by:

$$w_i^l(x, y, z) = \frac{z-z_i}{r^2} \left(\frac{1}{2\pi r} + \frac{1}{j\lambda} \right) \exp\left(\frac{j2\pi r}{\lambda}\right) \quad (3)$$

where $r = \sqrt{(x-x_i)^2 + (y-y_i)^2 + (z-z_i)^2}$ and $j = \sqrt{-1}$. Treating the input plane as the 0th layer, then for l^{th} layer ($l \geq 1$), the output field can be modeled as:

$$u_i^l(x, y, z) = w_i^l(x, y, z) \cdot t_i^l(x_i, y_i, z_i) \cdot \sum_k u_k^{l-1}(x_i, y_i, z_i) = w_i^l(x, y, z) \cdot |A| \cdot e^{j\Delta\theta}, \quad (4)$$

where $u_i^l(x, y, z)$ denotes the output of the i^{th} neuron on l^{th} layer located at (x, y, z) , the t_i^l denotes the complex modulation, i.e., $t_i^l(x_i, y_i, z_i) = a_i^l(x_i, y_i, z_i) \exp(j\phi_i^l(x_i, y_i, z_i))$. In eq. (4), $|A|$ is the relative amplitude of the secondary wave, and $\Delta\theta$ refers to the additional phase delay due to the input wave at each neuron, $\sum_k u_k^{l-1}(x_i, y_i, z_i)$, and the complex-valued neuron modulation function, $t_i^l(x_i, y_i, z_i)$.

Training loss function

To perform classification by means of all-optical diffractive networks with minimal post-processing (i.e., using only a *max* operation), we placed discrete detectors at the output plane. The number of detectors (D) is equal to the number of classes in the target dataset. The geometrical shape, location and size of these detectors ($6.4\lambda \times 6.4\lambda$) were determined before each training session. Having set the detectors at the output plane, the final loss value (L) of the diffractive neural network is defined through two different loss functions and their impact on D²NN based classifiers were explored (see the *Results* section). The first loss function was defined using the mean squared error (MSE) between the output plane intensity, S^{l+1} , and the target intensity distribution for the corresponding label, G^{l+1} , i.e.,

$$L = \frac{1}{K} \sum_i^K (S_i^{l+1} - G_i^{l+1})^2, \quad (5)$$

where K refers to the total number of sampling points representing the entire diffraction pattern at the output plane.

The second loss function used in combination with our all-optical D²NN framework is the cross-entropy. To use the cross-entropy loss function, an additional *softmax* layer is introduced and applied on the detected intensities (only during the training phase of a diffractive neural network design). With I_l denoting the total optical signal impinging onto the l^{th} detector at the output plane, the cross-entropy loss function can be written as follows:

$$L = - \sum_l^D g_l \log(p_l), \quad (6)$$

where $p_l = \frac{e^{l_l}}{\sum_l^D e^{l_l}}$ and g_l refer to the l^{th} element in the output of the *softmax* layer, and the l^{th} element of the ground truth label vector, respectively.

A key difference between the two loss functions is already apparent from eq. (5) and eq. (6).

While the MSE loss function is acting on the entire diffraction signal at the output plane of the diffractive network, the *softmax-cross-entropy* is applied to the detected optical signal values ignoring the optical field distribution outside of the detectors (one detector is assigned per class).

This approach based on *softmax-cross-entropy* loss brings additional degrees-of-freedom to the diffractive neural network training process, boosting the final classification performance as discussed in the *Results* section, at the cost of reduced diffraction efficiency and signal contrast at the output plane.

For the *all-electronic* neural network comparisons reported in Tables 1 and 2, the loss function used for the digital neural networks was based on *softmax-cross-entropy*.

Diffractive network training

All neural networks (optical and/or digital) were simulated using Python (v3.6.5) and TensorFlow (v1.10.0, Google Inc.) framework. All-optical, hybrid and electronic networks were trained for 50 epochs using a desktop computer with a GeForce GTX 1080 Ti Graphical Processing Unit, GPU and Intel(R) Core (TM) i9-7900X CPU @3.30GHz and 64GB of RAM, running Windows 10 operating system (Microsoft).

Two datasets were used in the training of the presented classifiers: MNIST and Fashion-MNIST. Both datasets have 70,000 objects/images, out of which we selected 55,000 and 5,000 as training

and validation sets, respectively. Remaining 10,000 were reserved as the test set. During the training phase, after each epoch we tested the performance of the current model in hand on the 5K validation set and upon completion of the 50th epoch, the model with the best performance on 5K validation set was selected as the final design of the network models. All the numbers reported in this work are blind testing accuracy results held by applying these selected models on the 10K test sets.

The trainable parameters in a diffractive neural network are the modulation values of each layer, which were optimized using a back-propagation method by applying the adaptive moment estimation optimizer (Adam)³³ with a learning rate of 1×10^{-3} . We chose a diffractive layer size of 200×200 neurons per layer, which were initialized with π for phase values and 1 for amplitude values. The training time was approximately 5 hours for a 5-layer D^2NN design with the hardware outlined above.

D^2NN -based hybrid network design

To further explore the potentials of D^2NN framework, we co-trained diffractive network layers together with digital neural networks to form hybrid systems. To begin with, keeping the optical architecture and the detector arrangement at the output plane of the diffractive network the same, a single fully-connected layer was introduced as an additional component (replacing the simplest *max* operations in an all-optical network), which maps the optical signal values coming from D individual detectors into a vector of the same size (i.e., the number of classes in the dataset). Since there are 10 classes in both MNIST and Fashion-MNIST datasets, this simple fully-connected digital structure brings additional 110 trainable variables (i.e., 100 coefficients in the weight matrix and 10 bias terms) into our hybrid system.

We then studied the impact of different detector configurations, by increasing the number of detectors forming an opto-electronic detector array, with a size of 10×10 , 25×25 and 50×50 pixels. Having different pixel sizes (see Table 3), all the three configurations (10×10 , 25×25 and 50×50 pixels) cover the central region of approximately $53.3\lambda\times 53.3\lambda$ at the output plane of the D^2NN . These different configurations were jointly-trained with multiple digital network architectures, simulating different hybrid systems. For the digital part, we focused on four different networks: a single fully-connected layer, 4-layer CNN, LeNet²⁵ and ResNet³¹ with 50 layers. The single fully-connected layer connects every pixel with 10 output classes, providing as few as 1,000 trainable parameters (see Table 3 for details). The 4-layer CNN has 2 convolutional layers with filter depth equal to 1, and 2 fully connected layers with 30 and 10 neurons; its architecture with respect to the input size is shown in Table 4. The LeNet architecture requires a certain input size of 32×32 pixels, thus the detector array values were resized using bilinear interpolation before being fed into the neural network. The ResNet architecture was only jointly-trained using the 50×50 pixel detector configuration, the output of which was resized using bilinear interpolation to 224×224 pixels before being fed into the network. The loss function of the D^2NN -based hybrid system was calculated by cross-entropy, evaluated at the output of the digital neural network. The training procedure was similar to the all-optical D^2NN designs.

References

- (1) Caulfield, H. J.; Kinser, J.; Rogers, S. K. Optical Neural Networks. *Proc. IEEE* **1989**, *77* (10), 1573–1583.
- (2) Yu, F. T. S.; Jutamulia, S. *Optical Signal Processing, Computing, and Neural Networks*, 1st ed.; John Wiley & Sons, Inc.: New York, NY, USA, 1992.
- (3) Yu, F. T. S. II Optical Neural Networks: Architecture, Design and Models. In *Progress in Optics*; Wolf, E., Ed.; Elsevier, 1993; Vol. 32, pp 61–144.
- (4) Psaltis, D.; Farhat, N. Optical Information Processing Based on an Associative-Memory Model of Neural Nets with Thresholding and Feedback. *Opt. Lett.* **1985**, *10* (2), 98–100.
- (5) Farhat, N. H.; Psaltis, D.; Prata, A.; Paek, E. Optical Implementation of the Hopfield Model. *Appl. Opt.* **1985**, *24* (10), 1469–1475.
- (6) Wagner, K.; Psaltis, D. Multilayer Optical Learning Networks. *Appl. Opt.* **1987**, *26* (23), 5061–5076.
- (7) Psaltis, D.; Brady, D.; Wagner, K. Adaptive Optical Networks Using Photorefractive Crystals. *Appl. Opt.* **1988**, *27* (9), 1752–1759.
- (8) Psaltis, D.; Brady, D.; Gu, X.-G.; Lin, S. Holography in Artificial Neural Networks. *Nature* **1990**, *343* (6256), 325–330.
- (9) Weverka, R. T.; Wagner, K.; Saffman, M. Fully Interconnected, Two-Dimensional Neural Arrays Using Wavelength-Multiplexed Volume Holograms. *Opt. Lett.* **1991**, *16* (11), 826–828.
- (10) Javidi, B.; Li, J.; Tang, Q. Optical Implementation of Neural Networks for Face Recognition by the Use of Nonlinear Joint Transform Correlators. *Appl. Opt.* **1995**, *34* (20), 3950–3962.
- (11) Shastri, B. J.; Tait, A. N.; de Lima, T. F.; Nahmias, M. A.; Peng, H.-T.; Prucnal, P. R. Principles of Neuromorphic Photonics. *ArXiv180100016 Phys.* **2018**, 1–37.
- (12) Shen, Y.; Harris, N. C.; Skirlo, S.; Prabhu, M.; Baehr-Jones, T.; Hochberg, M.; Sun, X.; Zhao, S.; Larochelle, H.; Englund, D.; et al. Deep Learning with Coherent Nanophotonic Circuits. *Nat. Photonics* **2017**, *11* (7), 441–446.
- (13) Bueno, J.; Maktoobi, S.; Froehly, L.; Fischer, I.; Jacquot, M.; Larger, L.; Brunner, D. Reinforcement Learning in a Large-Scale Photonic Recurrent Neural Network. *Optica* **2018**, *5* (6), 756–760.
- (14) Hughes, T. W.; Minkov, M.; Shi, Y.; Fan, S. Training of Photonic Neural Networks through in Situ Backpropagation and Gradient Measurement. *Optica* **2018**, *5* (7), 864–871.
- (15) Lin, X.; Rivenson, Y.; Yardimci, N. T.; Veli, M.; Luo, Y.; Jarrahi, M.; Ozcan, A. All-Optical Machine Learning Using Diffractive Deep Neural Networks. *Science* **2018**, *361* (6406), 1004–1008.
- (16) Chang, J.; Sitzmann, V.; Dun, X.; Heidrich, W.; Wetzstein, G. Hybrid Optical-Electronic Convolutional Neural Networks with Optimized Diffractive Optics for Image Classification. *Sci. Rep.* **2018**, *8* (1), 12324.
- (17) Soures, N.; Steidle, J.; Preble, S.; Kudithipudi, D. Neuro-MMI: A Hybrid Photonic-Electronic Machine Learning Platform. In *2018 IEEE Photonics Society Summer Topical Meeting Series (SUM)*; 2018; pp 187–188.
- (18) Chakraborty, I.; Saha, G.; Sengupta, A.; Roy, K. Toward Fast Neural Computing Using All-Photonic Phase Change Spiking Neurons. *Sci. Rep.* **2018**, *8* (1), 12980.
- (19) Bagherian, H.; Skirlo, S.; Shen, Y.; Meng, H.; Ceperic, V.; Soljacic, M. On-Chip Optical Convolutional Neural Networks. *ArXiv180803303 Cs* **2018**.
- (20) Tait, A. N.; de Lima, T. F.; Zhou, E.; Wu, A. X.; Nahmias, M. A.; Shastri, B. J.; Prucnal, P. R. Neuromorphic Photonic Networks Using Silicon Photonic Weight Banks. *Sci. Rep.* **2017**, *7* (1).
- (21) Mehrabian, A.; Al-Kabani, Y.; Sorger, V. J.; El-Ghazawi, T. PCNNA: A Photonic Convolutional Neural Network Accelerator. *ArXiv180708792 Cs Eess* **2018**.

- (22) George, J.; Amin, R.; Mehrabian, A.; Khurgin, J.; El-Ghazawi, T.; Prucnal, P. R.; Sorger, V. J. Electrooptic Nonlinear Activation Functions for Vector Matrix Multiplications in Optical Neural Networks. In *Advanced Photonics 2018 (BGPP, IPR, NP, NOMA, Sensors, Networks, SPPCom, SOF)*; OSA: Zurich, 2018; p SpW4G.3.
- (23) LeCun, Y.; Bengio, Y.; Hinton, G. Deep Learning. *Nature* **2015**, *521* (7553), 436–444.
- (24) Schmidhuber, J. Deep Learning in Neural Networks: An Overview. *Neural Netw.* **2015**, *61* (Supplement C), 85–117.
- (25) Lecun, Y.; Bottou, L.; Bengio, Y.; Haffner, P. Gradient-Based Learning Applied to Document Recognition. *Proc. IEEE* **1998**, *86* (11), 2278–2324.
- (26) Xiao, H.; Rasul, K.; Vollgraf, R. Fashion-MNIST: A Novel Image Dataset for Benchmarking Machine Learning Algorithms. *ArXiv170807747 Cs Stat* **2017**.
- (27) Maas, A. L.; Hannun, A. Y.; Ng, A. Y. Rectifier Nonlinearities Improve Neural Network Acoustic Models. In *Proc. icml*; 2013; Vol. 30, p 3.
- (28) Tang, Y. Deep Learning Using Linear Support Vector Machines. *ArXiv13060239 Cs Stat* **2013**.
- (29) Wan, L.; Zeiler, M.; Zhang, S.; Le Cun, Y.; Fergus, R. Regularization of Neural Networks Using Dropconnect. In *International Conference on Machine Learning*; 2013; pp 1058–1066.
- (30) Golik, P.; Doetsch, P.; Ney, H. Cross-Entropy vs. Squared Error Training: A Theoretical and Experimental Comparison. In *Interspeech*; 2013; Vol. 13, pp 1756–1760.
- (31) He, K.; Zhang, X.; Ren, S.; Sun, J. Identity Mappings in Deep Residual Networks. In *Computer Vision – ECCV 2016*; Leibe, B., Matas, J., Sebe, N., Welling, M., Eds.; Lecture Notes in Computer Science; Springer International Publishing, 2016; pp 630–645.
- (32) Goodman, J. W. *Introduction to Fourier Optics*; Roberts and Company Publishers, 2005.
- (33) Kingma, D. P.; Ba, J. Adam: A Method for Stochastic Optimization. *ArXiv E-Prints* **2014**, *1412*, arXiv:1412.6980.

Tables

All-Optical

	$\Delta_z = 40 \times \lambda$	$\Delta_z = 4 \times \lambda$
Phase only	97.18	94.12
Complex	97.81	96.01

Hybrid Systems

# of detectors	Optical Modulation	Digital Neural Networks							
		Single FC Layer		4-Layer CNN		LeNet		ResNet	
10	Phase only	97.65	93.12	N/A	N/A	N/A	N/A	N/A	N/A
	Complex	98.02	95.96	N/A	N/A	N/A	N/A	N/A	N/A
10×10	Phase only	98.23	98.17	98.22	97.98	98.31	98.53	N/A	N/A
	Complex	98.07	98.51	97.87	98.16	98.42	98.56	N/A	N/A
25×25	Phase only	98.28	98.06	98.47	98.25	98.70	98.34	N/A	N/A
	Complex	98.33	97.90	98.45	98.39	98.37	98.74	N/A	N/A
50×50	Phase only	98.22	98.36	98.57	98.45	98.42	98.49	98.38	99.02
	Complex	98.35	98.19	98.32	98.49	98.71	98.45	98.43	99.16

All Electronic

91.68	95.08	98.77	99.51
Single FC Layer	4-Layer CNN	LeNet	ResNet

Table 1. Blind testing accuracies (reported in percentage) for all-optical, hybrid and all-electronic networks used in this work for MNIST dataset. In the D²NN-based hybrid networks reported here, 4 different digital neural networks spanning from a single fully-connected layer to ResNet were co-trained with a D²NN design, placed before the electronic neural network. All the electronic neural networks used ReLU as the nonlinear activation function, and all the D²NN designs were based on spatially and temporally coherent illumination and linear optical materials,

with 5 diffractive layers. For a discussion on methods to incorporate optical nonlinearities in a diffractive neural network, refer to Ref. 15. Yellow and blue colors refer to $\Delta_z = 40\times\lambda$ and $\Delta_z = 4\times\lambda$, respectively.

All-Optical									
		$\Delta_z = 40\times\lambda$	$\Delta_z = 4\times\lambda$						
Phase only		87.67	85.98						
Complex		88.76	88.54						

Hybrid Systems									
# of detectors	Optical Modulation	Digital Neural Networks							
		Single FC Layer		4-Layer CNN		LeNet		ResNet	
10	Phase only	88.40	85.54	N/A	N/A	N/A	N/A	N/A	N/A
	Complex	88.69	88.84	N/A	N/A	N/A	N/A	N/A	N/A
10×10	Phase only	88.67	89.90	89.05	88.95	88.66	89.56	N/A	N/A
	Complex	88.82	89.60	89.02	88.93	89.25	89.68	N/A	N/A
25×25	Phase only	88.88	89.37	88.71	88.63	88.27	89.64	N/A	N/A
	Complex	89.45	89.82	89.06	88.80	89.03	89.79	N/A	N/A
50×50	Phase only	88.98	89.55	88.23	88.39	88.28	89.20	88.22	88.94
	Complex	89.34	89.84	88.94	88.55	87.81	89.27	88.59	88.98

All Electronic			
83.65	81.76	90.27	93.23
Single FC Layer	4-Layer CNN	LeNet	ResNet

Table 2. Blind testing accuracies (reported in percentage) for all-optical, hybrid and all-electronic networks used in this work for Fashion-MNIST dataset. In the D²NN-based hybrid networks reported here, 4 different digital neural networks spanning from a single fully-

connected layer to ResNet were co-trained with a D²NN design, placed before the electronic neural network. All the electronic neural networks used ReLU as the nonlinear activation function, and all the D²NN designs were based on spatially and temporally coherent illumination and linear materials, with 5 diffractive layers. For a discussion on methods to incorporate optical nonlinearities in a diffractive neural network, refer to Ref. 15. Yellow and blue colors refer to $\Delta_z = 40\times\lambda$ and $\Delta_z = 4\times\lambda$, respectively.

Detector configuration		The number of trainable parameters in the digital network			
Detector grid	Pixel size	Single FC layer	4-layer CNN	LeNet	ResNet
10×10	5.33λ×5.33λ	1000	2745	60840	N/A
25×25	2.13λ×2.13λ	6250	4845		N/A
50×50	1.06λ×1.06λ	25000	30045		25.5×10 ⁶

Table 3. Implementation details and the number of trainable parameters for the D²NN-based hybrid networks reported in this work. These 4 digital neural networks are using ReLU as the nonlinear activation function at each neuron.

Layer Type	Network architecture							
	Conv layer 1			Conv layer 2			FC layer 1	FC layer 2
Activation	ReLU			ReLU			ReLU	Softmax
Detector configuration	kernel	Feature map	Stride	kernel	Feature map	Stride	Number of neurons	Number of neurons
10×10	6×6	1	1	3×3	1	1	30	10
25×25			2			2		
50×50			2			2		

Table 4. 4-layer CNN architecture used in this work. Also see Table 3 for other details and comparison to other electronic neural networks used in this work.

List of Figures:

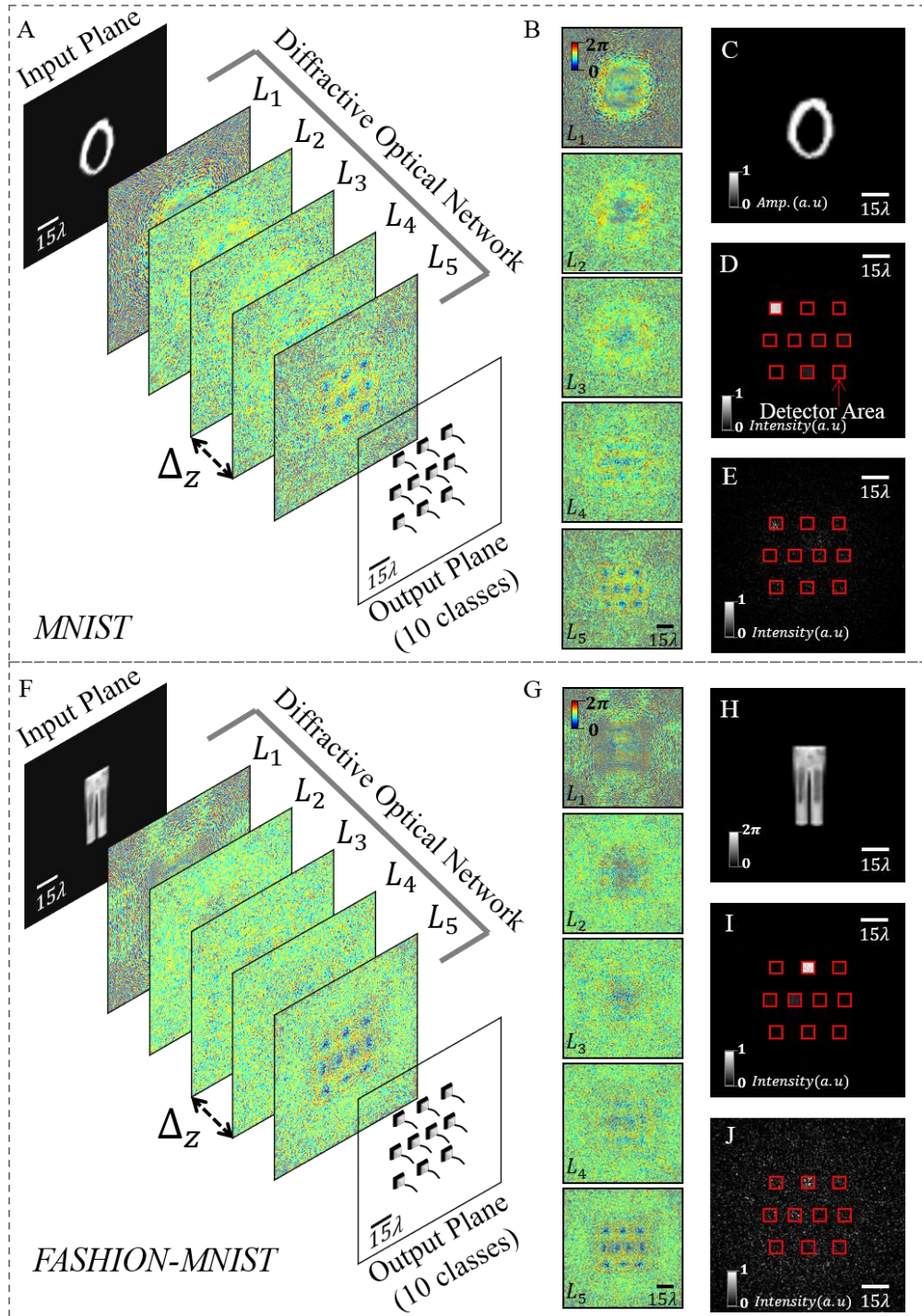


Figure 1. All-optical D²NN-based classifiers. These D²NN designs were based on spatially and temporally coherent illumination and linear optical materials/layers. (A) D²NN setup for the task

of classification of handwritten digits (MNIST), where the input information is encoded in the *amplitude* channel of the input plane. (B) Final design of a 5-layer, phase-only classifier for handwritten digits. (C) Amplitude distribution at the input plane for a test sample (digit '0'). (D-E) Intensity patterns at the output plane for the input in (C); (D) is for MSE-based, and (E) is softmax-cross-entropy (SCE)-based designs. (F) D²NN setup for the task of classification of fashion products (Fashion-MNIST), where the input information is encoded in the *phase* channel of the input plane. (G) Same as (B), except for fashion product dataset. (H) Phase distribution at the input plane for a test sample. (I-J) Same as (D) and (E) for the input in (H). λ refers to the illumination source wavelength. Input plane represents the plane of the input object or its data, which can also be generated by another optical imaging system or a lens, projecting an image of the object data onto this plane.

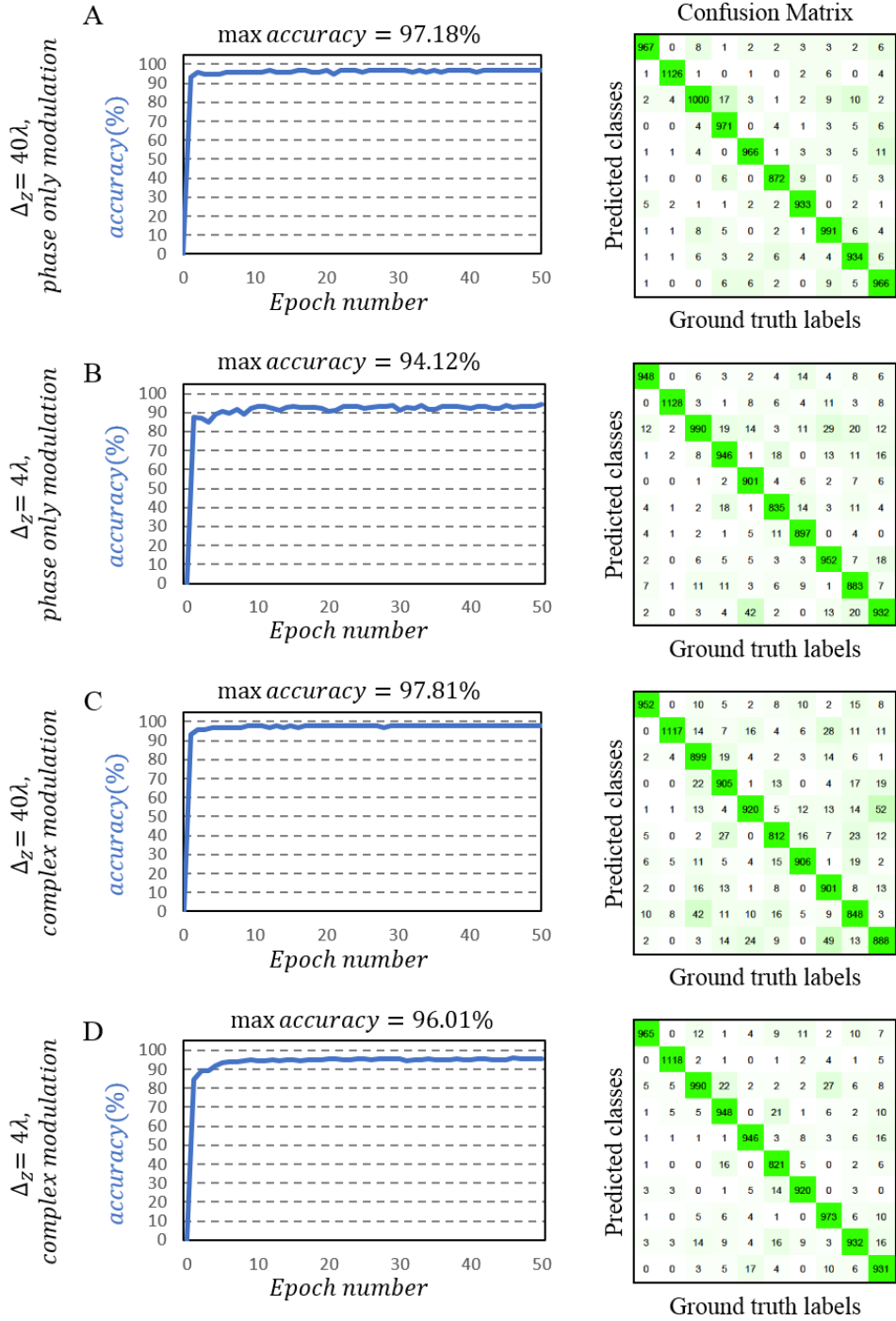


Figure 2. Convergence plots and confusion matrices for all-optical D^2 NN-based classification of handwritten digits (MNIST dataset). (A) Convergence curve and confusion matrix for a phase-only, fully-connected D^2 NN ($\Delta_z = 40\lambda$) design. (B) Convergence curve and confusion matrix for a phase-only, partially-connected D^2 NN ($\Delta_z = 4\lambda$) design. (C) and (D) are counterparts of (A)

and (B), respectively, for complex-modulation D^2NN designs, where both the amplitude and phase of each neuron are trainable parameters.

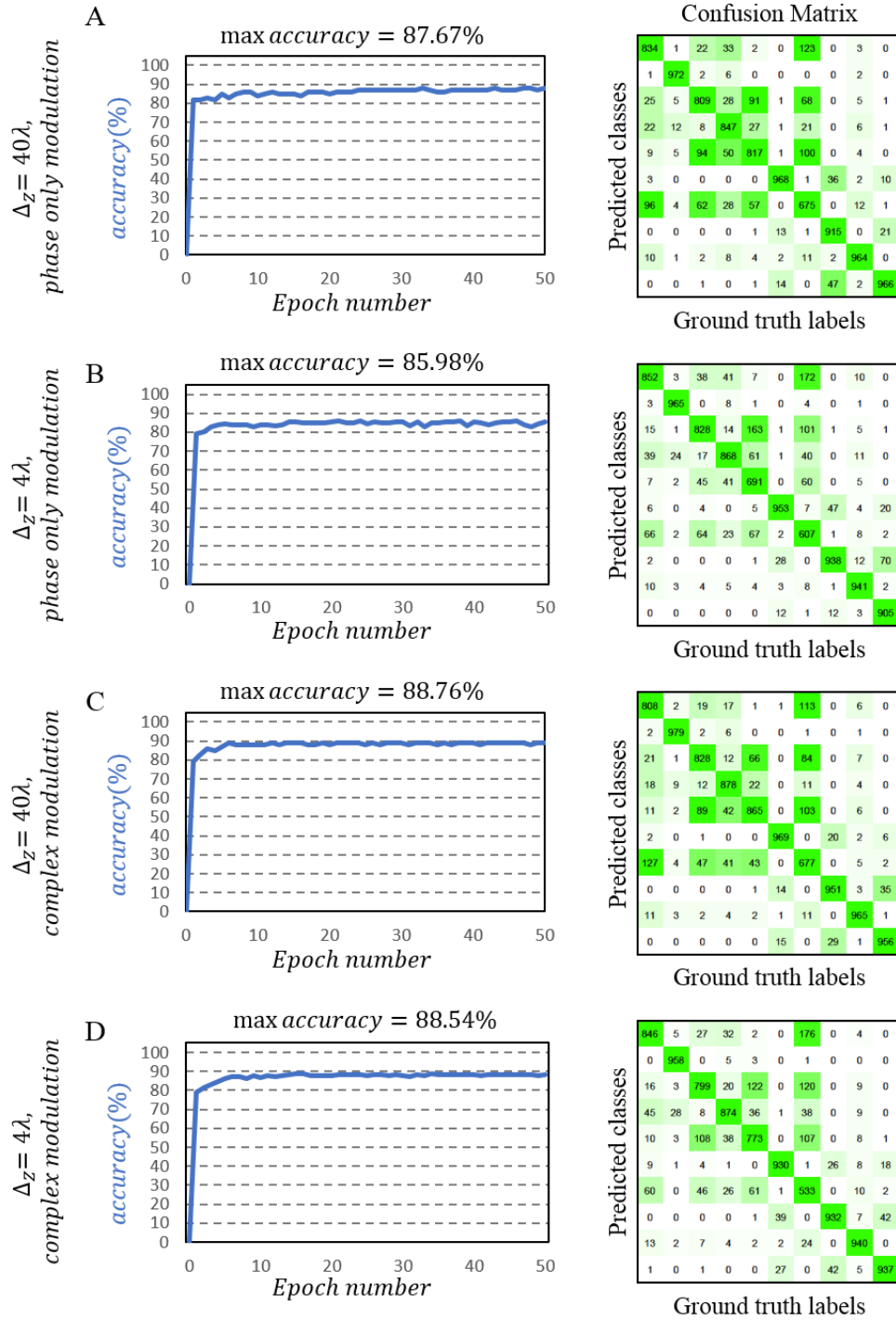


Figure 3. Same as Figure 2, except the results are for all-optical D²NN-based classification of fashion products (Fashion-MNIST dataset).

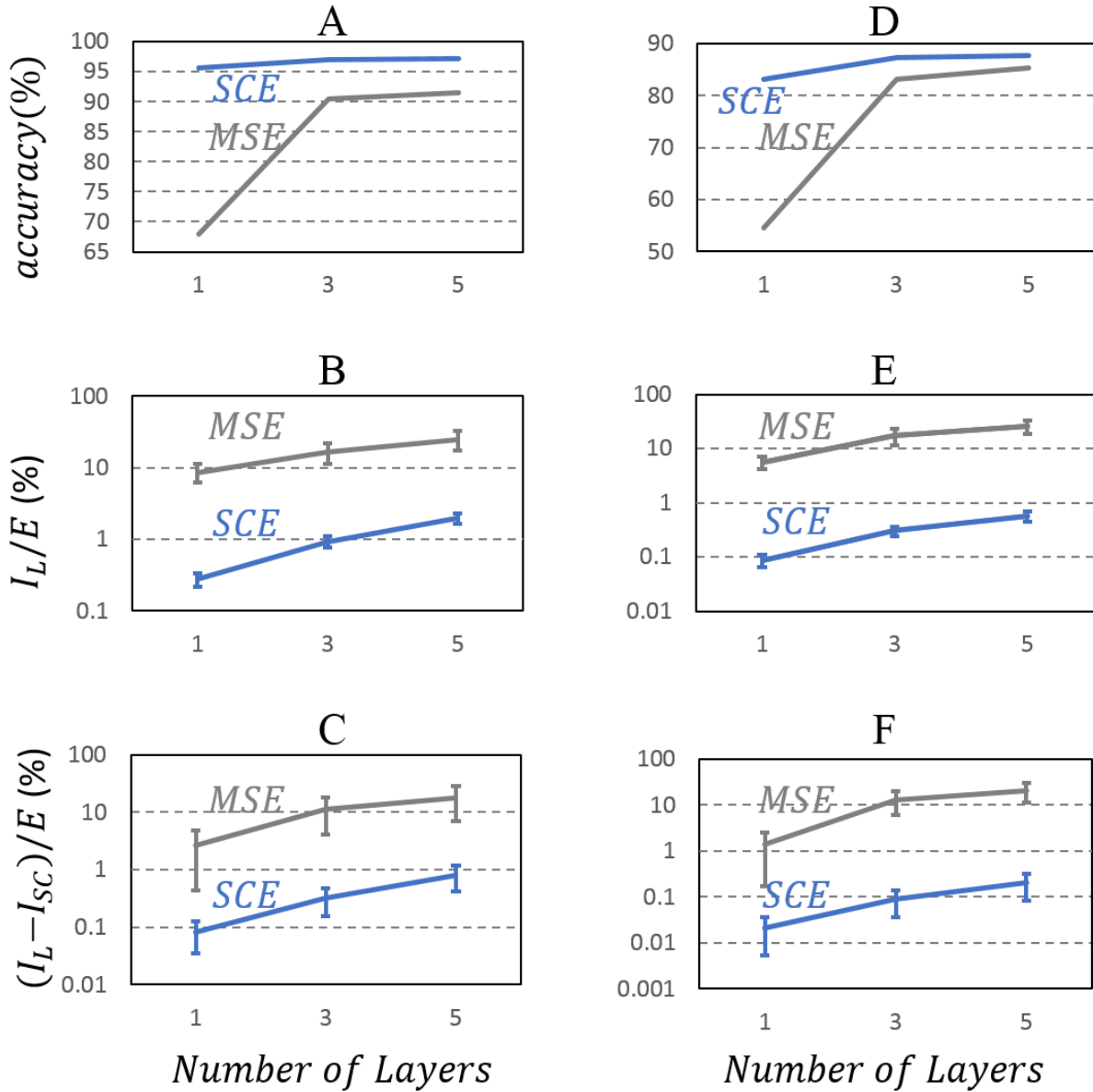


Figure 4. Classification accuracy, power efficiency and signal contrast comparison of MSE and SCE loss function based all-optical phase-only D^2 NN classifier designs with 1, 3 and 5-layers. (A) Blind testing accuracy, (B) power efficiency and (C) signal contrast analysis of the final design of fully-connected, phase-only all-optical classifiers trained for handwritten digits (MNIST). (D-F) are the same as (A-C), only the classified dataset is Fashion-MNIST instead.

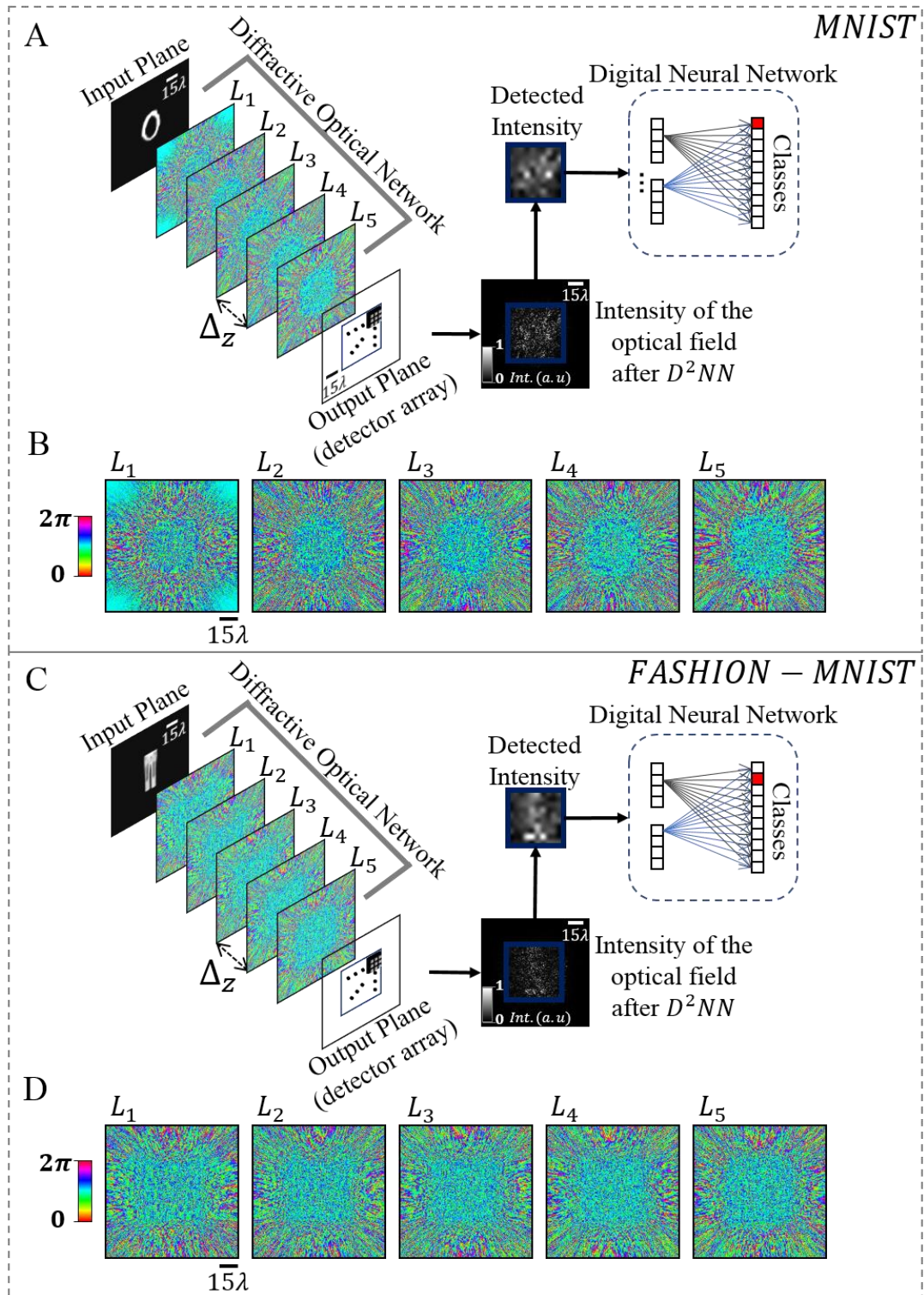


Figure 5. D^2NN -based hybrid neural networks. (A) The architecture of a hybrid (optical and electronic) classifier. (B) Final design of phase-only optical layers at the front-end of a hybrid

handwritten digit classifier with a 10×10 opto-electronic detector array at the bridge/junction between the two modalities (optical vs. electronic). (C) and (D) are same as (A) and (B), except the latter are for Fashion-MNIST dataset. Input plane represents the plane of the input object or its data, which can also be generated by another optical imaging system or a lens, projecting an image of the object data onto this plane.